Electrocatalysts

DOI: 10.1002/anie.201302090

Ultrathin PtPdTe Nanowires as Superior Catalysts for Methanol Electrooxidation**

*Hui-Hui Li, Shuo Zhao, Ming Gong, Chun-Hua Cui, Da He, Hai-Wei Liang, Liang Wu, and Shu-Hong Yu**

Lowering the costs without loss of the performance is still the obstacle for the commercialization of fuel cells.[1] To overcome the obstacle, advanced synthesis strategies have been developed and investigated to control size, shape, composition, and arrangement of surface atoms of the electrocatalysts.[2] One-dimensional (1D) motifs, especially ultrathin nanowires (NWs) with a diameter below 10 nm, exhibited improved surface chemistry and catalytic properties.[3] Obviously, the decrease in the size of the NWs leads to increased surface areas that provide more active sites and increase Pt utilization per mass.[4] For example, ultrathin and superlong Pt NWs demonstrated higher surface area, activity, and stability relative to Pt nanoparticles for the methanol oxidation reaction (MOR).[2g,5] And, the existence of single-crystalline segments (SCSs) of the NWs allowed for the preferential exposure of long segments with high crystallinity and low-energy crystal facets, which is highly advantageous for the electrocatalytic reactions.[5] The addition of a second or third metal (e.g., Pd, Au, Ag, Fe, Ni, Cu, Zn, Ru) to Pt to form Pt-based heteronanostructures or alloy catalysts could further decrease the Pt loading.[6] The unique alloyed NW catalysts with controlled architectures and compositions exhibited a superior activity in the MOR owing to the electronic effect and/or bifunctional mechanism.[7]

To date, most of the reported syntheses of Pt-based electrocatalysts have been achieved by colloid approaches and the electrodeposition method.[8] Sun and co-workers recently reported a one-pot synthesis of ultrathin ternary FePtPd alloy NWs by thermal decomposition of $[Fe(CO)_5]$ and sequential reduction of $[Pt(acac)_2]$ and $[Pd(acac)_2]$ (acac = acetylacetonate).[9] This catalyst exhibited an impressive mass activity of about 488.7 $mA\,mg^{-1}$ Pt. The enhancement of the activity of PtRh alloy nanocatalysts in the MOR in comparison with that of the commercial Pt E-TEK catalysts, reported by Zhang et al.,[10] was attributed to the combination of electronic and bifunctional effects. 1D PdAuCu, PtNi, and CuPt electrocatalysts with high activity were also prepared using electrodeposition.[11] Thus, the controlled synthesis of alloyed NW catalysts in large scale with low cost is still challenging but very attractive.

Herein, we report a facile route for the large-scale synthesis of uniform, ultrathin (diameter 5–7 nm), and ultralong (aspect ratio $>10^4$) PtPdTe and PtTe NWs in ethylene glycol (EG) solution by using Te NWs as both sacrificial templates and reducing agents. Fine-tuning of the molar ratios of Pt and Pd precursors afford PtPdTe NWs with controlled compositions. The optimal content of Pd atoms could produce the SCSs along the NWs and balance the electronic and bifunctional effects, which induce a higher activity toward the MOR in comparison with commercial Pt/C.

The high-quality ultrathin Te NWs (Figure S1 in the Supporting Information) were synthesized by using the method we developed previously.[12] The synthesis of pure Pt NWs and noble-metal alloy NWs has been reported using Te NWs as sacrificial templates. However, Pt or Pd precursors are always used in a 2–4-fold excess compared to Te to replace the Te NWs completely.[13] Here, the stoichiometric ratio of total noble-metal precursors to Te was only 0.2, at the expense of generating partial Te NWs, thereby greatly reducing the cost and dosage of Pt and Pd precursors during the synthesis process; thus PtPdTe NWs were prepared. Obviously, the Te NWs are only partially consumed according to the ratio between noble-metal precursors and Te NWs, thus our method could make full use of Te atoms in the NWs. More importantly, unreacted Te atoms alloying with PtPd to form PtPdTe NWs, support the NW skeleton and minimize the precious metal loading, which could impart enhanced catalytic performance. Thus, the present route provides a more source-saving and more environmentally friendly synthesis method compared with any previous approaches.[13]

Energy-dispersive X-ray spectroscopy (EDS) analysis on a random selection of PtPdTe NWs (Figure 1a and Supporting Information Figure S2) shows that the preparation methods allows tuning of the NW composition. By adding a fixed dosage of the total noble-metal precursors and tuning the molar ratios of K_2PtCl_4 or K_2PdCl_4, we prepared $Pt_{28}Pd_{15}Te_{57}$, $Pt_{23}Pd_{21}Te_{56}$, $Pt_{16}Pd_{31}Te_{53}$, and $Pt_{49}Te_{51}$ NWs

[*] H. H. Li, S. Zhao, Dr. C. H. Cui, D. He, Dr. H. W. Liang, L. Wu, Prof. Dr. S. H. Yu
Division of Nanomaterials & Chemistry, Hefei National Laboratory for Physical Sciences at Microscale, Department of Chemistry, University of Science and Technology of China
Hefei 230026 (P. R. China)
E-mail: shyu@ustc.edu.cn
Homepage: http://staff.ustc.edu.cn/~yulab
Prof. Dr. M. Gong
Engineering and Materials Science Experiment Center
University of Science and Technology of China
Hefei 230026 (P.R.China)

[**] S.H.Y. acknowledges the funding from the National Basic Research Program of China (Grant 2010CB934700), the National Natural Science Foundation of China (Grants 91022032, 91227103, 21061160492), the Chinese Academy of Sciences (Grant KJZD-EW-M01-1), the International Science & Technology Cooperation Program of China (Grant 2010DFA41170), and the Principal Investigator Award by the National Synchrotron Radiation Laboratory at the University of Science and Technology of China.

Supporting information for this article is available on the WWW under http://dx.doi.org/10.1002/anie.201302090.

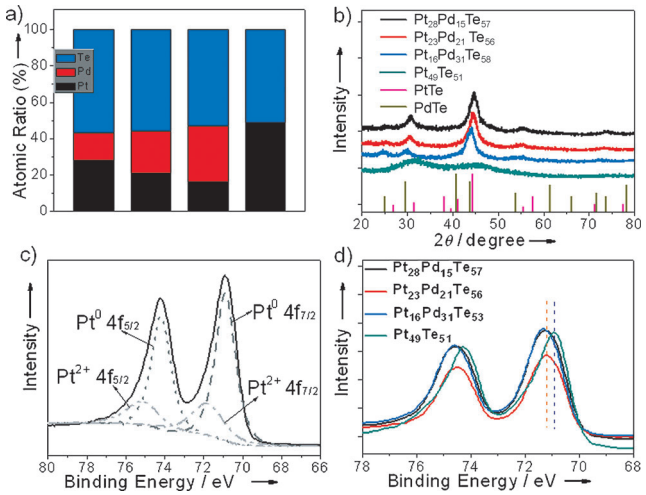

Figure 1. a) Variations in the Pt/Pd/Te ratio in the PtPdTe NWs determined by EDS owing to different dosages of the Pt and Pd precursors during the fabrication process. The precursor dosages are given in the Supporting Information. b) XRD patterns of the PtPdTe NWs with different component ratios. PtTe and PdTe data were obtained from JCPDS No. 15-0525 and 18-0954, respectively. c) High-resolution X-ray photoelectron spectroscopy (XPS) spectra of Pt 4f orbital of $Pt_{23}Pd_{21}Te_{56}$ NWs. d) Comparison of the XPS spectra of PtPdTe NWs with different component fractions.

under the same reaction conditions. These catalysts possess roughly an identical atomic faction of Te and the component ratios are close to the stoichiometric ratios of the applied precursors. The X-ray diffraction (XRD) patterns are shown in Figure 1b. The absence of pure Te, Pt, or Pd phases shows that the catalysts are ternary alloyed NWs. Each of the peaks of the PtPdTe NWs is located between the two corresponding peaks of PtTe and PdTe. Compared with those of the $Pt_{49}Te_{51}$ NWs, all the diffraction peaks of the PtPdTe NWs have lower diffraction angles, which further shift toward lower angles with increasing Pd content. Such a consistent shift also could be an evidence for the alloy formation among Pt, Pd, and Te.[14]

Figure 1c presents the Pt 4f core level spectra for $Pt_{23}Pd_{21}Te_{56}$ NWs. The Pt 4f core levels split into $4f_{5/2}$ and $4f_{7/2}$ states because of spin-orbital splitting. The binding energy (BE) values at 74.2 and 70.9 eV correspond to Pt $4f_{5/2}$ and Pt $4f_{7/2}$, respectively, which can be assigned to Pt^0 species. Two more peaks at 75.2 and 71.9 eV indicate the presence of Pt^{2+} species.[15] According to Pt^0/Pt^{2+} intensity ratio, the NWs were predominantly in the zero-valent state. In the high-resolution Te 3d XPS spectra for $Pt_{23}Pd_{21}Te_{56}$ NWs (Figure S3 in the Supporting Information), the BE values of 572.7 and 583.1 eV correspond to metallic Te^0 and those at 575.8 and 586.2 eV to oxidized Te^{4+}. The zero-valent Te proved the formation of alloy $Pt_{23}Pd_{21}Te_{56}$ NWs. The upshift of the binding energy for Pt after the inclusion of Pd atoms relative to the $Pt_{49}Te_{51}$ NWs (Figure 1d) results from the modification of electronic structures and a downshift of the d-band center position,[6c,14a] thus resulting in the decrease of the adsorption energy of CO on Pt.

Transmission electron microscopy (TEM) images of the $Pt_{23}Pd_{21}Te_{56}$ NWs reveal a narrow diameter distribution ranging from 5 to 7 nm (Figure 2a,b). The inset in Figure 2a shows the sucsesful large-scale (100 mg) synthesis of $Pt_{23}Pd_{21}Te_{56}$ NWs. The NWs with a length up to hundreds of nanometers are flexible and intertwisted with each other to form a NW network (Figure 2a). Interestingly, these NWs can easily form a film through a filtration process (Figure 2g) or

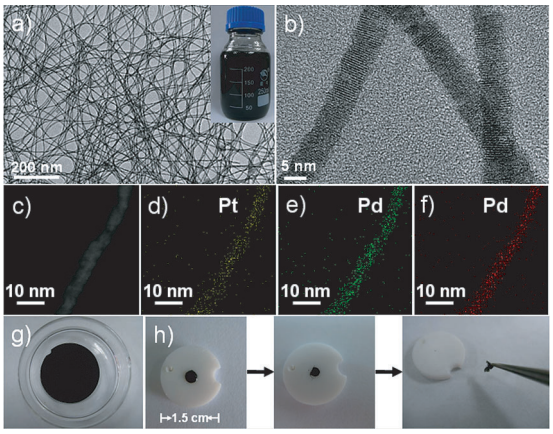

Figure 2. a) TEM image of the $Pt_{23}Pd_{21}Te_{56}$ NWs; b) magnified image of a part of (a). The inset in (a) is a photograph of an ethanol suspension of $Pt_{23}Pd_{21}Te_{56}$ NWs. c–f) HAADF-STEM characterization of $Pt_{23}Pd_{21}Te_{56}$ NWs. g) Photograph of a $Pt_{23}Pd_{21}Te_{56}$ NW film obtained through a filtration process. h) Photographs of a simple cast process of the formation of a $Pt_{23}Pd_{21}Te_{56}$ NW film on a teflon substrate.

a simple casting process (Figure 2h). When we add the $Pt_{23}Pd_{21}Te_{56}$ NW ethanol suspension on a teflon substrate, the film forms after the ethanol evaporated completely. In the same way, a thin film will form when the NWs are added on the glass–carbon rotating electrode (RDE) prior to electrocatalysis tests; the film would facilitate the effective mass transport of reactants and products.[13a,16]

The high-angle annular dark-field scanning TEM (HAADF-STEM) image of a $Pt_{23}Pd_{21}Te_{56}$ NW and the corresponding elemental mappings of Pt, Pd and Te are shown in Figure 2c–f. These elemental mappings indicate that all of the three elements were uniformly distributed in the NW. More importantly, there exist SCSs along the axis of the NWs with high crystallinity and low-energy crystal facets.[5]

The white circles shown in Figure 3 indicate the observed SCSs of the $Pt_{23}Pd_{21}Te_{56}$ NWs. The high-resolution (HR) TEM images (Figure 3c–j) show the majority of the SCSs have lattice spacings of 0.289 nm. The TEM and HRTEM images of $Pt_{28}Pd_{15}Te_{57}$, $Pt_{16}Pd_{31}Te_{53}$, and $Pt_{49}Te_{51}$ NWs with the same structural features are shown in Figures S4–S6 in the Supporting Information, respectively. Ultralong $Pt_{28}Pd_{15}Te_{57}$ NWs distribute uniformly with a diameter between 5 and 7 nm (Figure S4) and SCSs exist along the NWs (Figure S4c), as well as in $Pt_{16}Pd_{31}Te_{53}$ NWs (Figure S5). However, there are only few SCSs along the $Pt_{49}Te_{51}$ NWs (Figure S6). So, the existence of Pd atoms in the alloy NWs is an important factor to form SCSs, which could be greatly advantageous for the electrocatalytic activity, and the Te atoms retained in the NWs will minimize the loading of the precious metals.

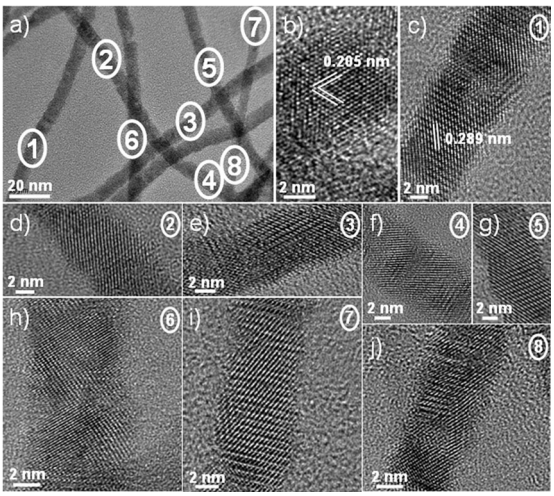

Figure 3. a) The white circles indicate the observed SCSs of $Pt_{23}Pd_{21}Te_{56}$ NWs. b–j) HRTEM images of the $Pt_{23}Pd_{21}Te_{56}$ NWs. The HRTEM images in (c–j) obtained along the SCSs with a spacing of 0.289 nm correspond to the marked numbers in (a).

The electrochemical properties of the PtPdTe NWs were studied by cyclic voltammetry (CV). The cyclic voltammograms of the $Pt_{23}Pd_{21}Te_{56}$ NWs were obtained in Ar-saturated H_2SO_4 (0.5 M) solution at 250 $mV\,s^{-1}$ (for the first and the 20th cycle see Figure S7 in the Supporting Information). CV is a technology to study the surface chemistry of catalysts during dealloying. A PtPd-enriched surface was obtained after the voltammetric dealloying procedure, which could improve the exposure of active Pt and Pd sites, improve Pt utilization, and allow lower Pt loading.[17] Meanwhile, the potential cycling could rearrange surface Pt and Pd atoms owing to the dissolution of neighboring Te atoms and activate the surface sites.[18]

The peak between 0.6–0.9 V in the first cycle indicated the dissolution of Te atoms from the surface of the $Pt_{23}Pd_{21}Te_{56}$ NWs in the acidic environment,[19] thereby inducing a PtPd-enriched surface of the NWs and further improving electron conduction between the surface sites. The intensity of the dissolution peaks of Te atoms decreased in the following cycling. Simultaneously, the increase in underpotential deposited hydrogen (H_{upd}) between −0.2 and 0.15 V suggests the exposure of a PtPd-enriched surface. This could also be proved by the relative composition difference before and after cycling, both in the bulk and the surface of the samples. The atomic fraction of Te decreased from 56 % to 8.3 % in the bulk (Figure S8 in the Supporting Information) owing to Te leaching. The Pt/Pd atomic ratio remains unchanged compared with the ratio before the treatment. The XPS data demonstrated that there are few Te atoms in the surface. The atomic fraction of the sum of Pt and Pd in the surface is higher than that in the bulk, which proved the formation of NWs with a PtPd-enriched surface. Additionally, TEM images of the PtPd-enriched NWs were taken after the dealloying process (Figure S9 in the Supporting Information). An ultrathin film could be easily formed (Figure S9a). More importantly, TEM and HRTEM images show that the SCSs were retained after the leaching of Te atoms, implying the stable structure in morphology (Figure S10 in the Supporting Information).

The composition effects of the PtPdTe NWs on the activity in the MOR are studied in H_2SO_4 (0.5 M) and methanol (1.0 M) solutions at a sweep rate of 50 $mV\,s^{-1}$, and the activities are compared with those of the $Pt_{49}Te_{51}$ NWs and commercial Pt/C catalysts measured under the same conditions (Figure 4a). The calculation of the electrochemically

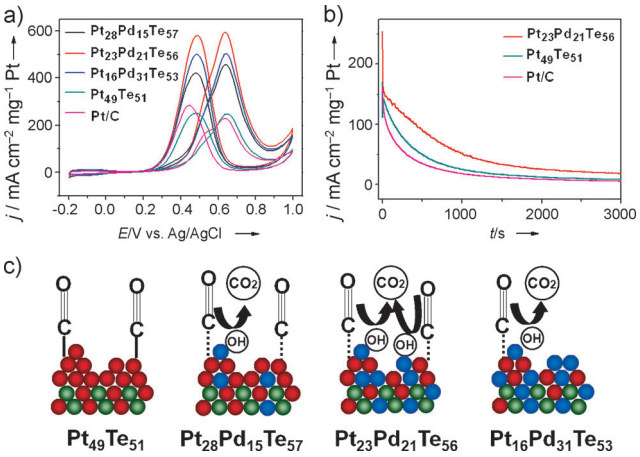

Figure 4. a) Cyclic voltammetric curves of PtPdTe NWs, $Pt_{49}Te_{51}$ NWs, and Pt/C catalysts for the MOR in 0.5 M H_2SO_4 + 1.0 M methanol solution at a sweep rate of 50 $mV\,s^{-1}$. b) Chronoamperograms for the MOR at 0.5 V vs. Ag/AgCl of $Pt_{23}Pd_{21}Te_{56}$ NWs, $Pt_{49}Te_{51}$ NWs, and Pt/C catalysts in 0.5 M H_2SO_4 + 1.0 M methanol solution. The current density is normalized in reference to the real Pt surface areas per mass. c) Illustration of the CO adsorbed on the $Pt_{49}Te_{51}$, $Pt_{28}Pd_{15}Te_{57}$, $Pt_{23}Pd_{21}Te_{56}$, and $Pt_{16}Pd_{31}Te_{53}$ NWs and the formation of Pd–OH at low potential to activate the oxidation of CO to produce CO_2. The bonding (dashed lines) of Pt–CO in PtPdTe NWs is weaker than that (solid lines) of Pt–CO in $Pt_{49}Te_{51}$ NWs owing to the modified electronic structure of Pt. Red, blue, and green represent Pt, Pd, and Te atoms, respectively. The atom arrangement is in accordance with the atomic ratios of Pt/Te or Pt/Pd/Te of the NWs.

active surface area (ECSA) is described in detail in the Supporting Information. The catalytic activity for the MOR was normalized to the real surface area per mass. Among the three kinds of PtPdTe NWs, the $Pt_{23}Pd_{21}Te_{56}$ NWs exhibit the highest electrocatalytic activity at 595.0 $mA\,cm^{-2}\,mg^{-1}$ Pt, which is 2.4- and 2.6-fold higher than that of $Pt_{49}Te_{51}$ NWs (249.8 $mA\,cm^{-2}\,mg^{-1}$ Pt) and Pt/C (229.0 $mA\,cm^{-2}\,mg^{-1}$ Pt) catalysts, respectively. The peak current ratio of the forward scan (I_f) to backward scan (I_b), I_f/I_b, could represent the ability of resistence to the poisoning of carbonaceous species.[11c] The I_f/I_b of the $Pt_{23}Pd_{21}Te_{56}$ NWs is 1.02, which is a little higher than that of $Pt_{49}Te_{51}$ NWs and 1.27 times higher than that of Pt/C catalysts (0.8). $Pt_{51}Pd_{49}$ NWs that have the same Pt/Pd atomic ratio as the $Pt_{23}Pd_{21}Te_{56}$ NWs were also synthesized by replacing the Te from the template Te NWs completely. The morphology of the $Pt_{51}Pd_{49}$ NWs is similar to that of PtPdTe NWs, as shown by the TEM images in Figure S11 in the Supporting Information. The atomic ratio of Pt and Pd was confirmed by inductively coupled plasma mass spectrometry (ICP). The $Pt_{23}Pd_{21}Te_{56}$ NWs show a much higher activity than

$Pt_{51}Pd_{49}$ NWs (336.8 mA cm^{-2} mg^{-1} Pt) with the same Pt loading (Figure S12 in the Supporting Information). According to the ratio I_f/I_b, the $Pt_{23}Pd_{21}Te_{56}$ NWs also have an improved poison tolerance. These results proved that more active surface sites per mass and higher noble-metal utilization can be obtained by the $Pt_{23}Pd_{21}Te_{56}$ NWs owing to the initial exsitence of Te atoms.

Chronoamperometric curves (Figure 4b) were recorded at 0.5 V vs. Ag/AgCl for 3000 s to evalutate the stability of the electroctatalysts. The chronoamperometry generates high charging currents owing to the initial high concentration of methanol on the surface of the electrocatalysts, but at the initial stage the current intensity decays rapidly because of the decrease of the concentration gradient and poisoning by the intermediate species. According to Figure S13 in the Supporting Information (chronoamperometry curves only for the initial 600 s from Figure 4b), we find that the current density induced by our catalysts decays more slowly than that by commercial Pt/C at the initial 600 s. Clearly, our catalysts exhibit a much higher activity than commercial Pt/C. These results are consistent with the reported results, which show the stability tests for initial 200 s.[13b] And the long-term poisoning rate of the $Pt_{23}Pd_{21}Te_{56}$ NWs and Pt/C catalysts are 0.02 and 0.03 % s^{-1}, respectively, which can be calculated by measuring the linear decay of the current (see the Supporting Information for details).[20] The $Pt_{23}Pd_{21}Te_{56}$ NWs always exhibited a lower deterioration rate than the Pt/C catalysts over the entire time range shown in Figure 4b, confirming their enhanced stability. These results are also consistent with that (stability tests for 2000 s) reported by Yamauchi and coworkers.[16]

In comparison with the commercial Pt/C and $Pt_{49}Te_{51}$ NW catalysts, the addition of Pd atoms in the PtPdTe NWs provides great opportunities to enhance their catalytic activity and stability owing to the existence of SCSs and a combination of the electronic effect and the bifunctional mechanism. The optimal content of Pd atoms in the NWs catalysts could maximize both electroactivity and stability of the PtPdTe NWs relative to $Pt_{49}Te_{51}$ NWs, and the origin of the enhanced catalytic properties can be explained by the modification of the electronic effect and the bifunctional mechanism (Figure 4c). For the electronic effect, the electronic structure of Pt modified by adjacent Pd atoms, proved by XPS, could decrease the CO adsorption energy and favor C–H cleavage on Pt sites owing to the shift of the d-band center.[21] Thus, the PtPdTe NWs could remove the CO intermediates easier than $Pt_{49}Te_{51}$ NWs. For the bifunctional mechanism, Pt preferably catalyzes methanol dehydrogenation to form Pt–CO, while the dissociative adsorption of water molecules occurs favorably on the Pd sites to form Pd–OH, which is believed to activate CO oxidation to produce CO_2 and release the active metal surface sites.[22] On Pd-free, like $Pt_{49}Te_{51}$, catalysts, the formation of Pt–OH needs a higher potential,[15,22a] making the overall oxidation process on Pt-rich surfaces sluggish. At a low content of Pd, like in $Pt_{28}Pd_{15}Te_{57}$ NWs catalysts, there may be insufficient Pd sites for the water dehydrogenation to form Pd–OH that facilitate the oxidization of CO. At a higher content of Pd, like in $Pt_{16}Pd_{31}Te_{53}$ NWs catalysts, less Pt sites would make the overall reaction more sluggish owing to the suppression in methanol dehydrogenation. Therefore, the optimal Pt and Pd content in the electrocatalysts could balance these effects to obtain an optimal electrocatalytic activity.

In conclusion, we have developed a simple method to produce high-yield, uniform, ultralong, and ultrathin PtPdTe NWs with controlled composition and SCSs. The unique structural features are greatly advantageous for enhancement of the MOR. In the synthesis, the ratio of the total noble-metal precursors to Te is only 0.2, thus greatly decreasing the cost. The retained Te atoms in the nanowires alloyed with Pt and Pd to form PtPdTe NWs, thus maintained the nanowire structures and minimized the noble-metal loading. The presence of Pd atoms also plays a key role in improving the catalytic activity, because it is important for both the modification of the electronic structure of Pt and the formation of Pd–OH at low potentials by breaking water molecules. An optimal Pd content is required to balance the elelctronic effect and the bifunctional effect. This composition–property correlation is ascribed from the ratio, arrangement of PtPd, and the increased number of available active Pt and Pd sites in the surface of the PtPdTe NWs. The present method provides a promising and alternative approach for the design of new MOR electrocatalysts with high performance in the future.

Received: March 13, 2013
Revised: April 26, 2013
Published online: June 6, 2013

Keywords: electrocatalysts · heterogeneous catalysis · methanol oxidation · nanowires · platinum

[1] S. Chu, A. Majumdar, *Nature* **2012**, *488*, 294 – 303.
[2] a) M. K. Debe, *Nature* **2012**, *486*, 43 – 51; b) S. H. Yu, F. Tao, J. Liu, *ChemCatChem* **2012**, *4*, 1445 – 1447; c) C. H. Cui, S. H. Yu, *Acc. Chem. Res.* **2013**, DOI: 10.1021/ar300254b; d) B. Lim, M. J. Jiang, P. H. C. Camargo, E. C. Cho, J. Tao, X. M. Lu, Y. M. Zhu, Y. N. Xia, *Science* **2009**, *324*, 1302 – 1305; e) J. Zhang, C. M. Li, *Chem. Soc. Rev.* **2012**, *41*, 7016 – 7031; f) X. Shan, D. P. Ismael, L. J. Wang, P. Wiktor, Y. Gu, L. H. Zhang, W. Wang, J. Lu, S. P. Wang, Q. H. Gong, J. H. Li, N. J. Tao, *Nat. Nanotechnol.* **2012**, *7*, 668 – 672; g) L. G. Zhang, N. Li, F. M. Gao, L. Hou, Z. M. Xu, *J. Am. Chem. Soc.* **2012**, *134*, 11326 – 11329.
[3] a) H. W. Liang, J. W. Liu, H. S. Qian, S. H. Yu, *Acc. Chem. Res.* **2013**, DOI: 10.1021/ar300272m; b) J. W. Liu, H. W. Liang, S. H. Yu, *Chem. Rev.* **2012**, *112*, 4770 – 4799; c) L. Cademartiri, G. A. Ozin, *Adv. Mater.* **2009**, *21*, 1013 – 1020; d) C. Koenigsmann, S. S. Wong, *Energy Environ. Sci.* **2011**, *4*, 1161 – 1176.
[4] a) S. J. Guo, D. G. Li, H. Y. Zhu, S. Zhang, N. M. Markovic, V. R. Stamenkovic, S. H. Sun, *Angew. Chem.* **2013**, *125*, 3549 – 3552; *Angew. Chem. Int. Ed.* **2013**, *52*, 3465 – 3468; b) H. H. Li, C. H. Cui, S. H. Yu, *ChemCatChem* **2013**, DOI: 10.1002/cctc.201300155.
[5] a) C. Koenigsmann, E. Sutter, T. A. Chiesa, R. R. Adzic, S. S. Wong, *Nano Lett.* **2012**, *12*, 2013 – 2020; b) C. Koenigsmann, W. P. Zhou, R. R. Adzic, E. Sutter, S. S. Wong, *Nano Lett.* **2010**, *10*, 2806 – 2811.
[6] a) J. Greeley, I. E. L. Stephens, A. S. Bondarenko, T. P. Johansson, H. A. Hansen, T. F. Jaramillo, J. Rossmeisl, I. Chorkendorff, J. K. Nørskov, *Nat. Chem.* **2009**, *1*, 552 – 556; b) A. Kowal, M. Li, M. Shao, K. Sasaki, M. B. Vukmirovic, J. Zhang, N. S. Marin-

kovic, P. Liu, A. I. Frenkel, R. R. Adzic, *Nat. Mater.* **2009**, *8*, 325 – 330; c) V. R. Stamenkovic, B. S. Mun, M. Arenz, K. J. J. Mayrhofer, C. A. Lucas, G. F. Wang, P. N. Ross, N. M. Markovic, *Nat. Mater.* **2007**, *6*, 241 – 247; d) C. H. Cui, H. H. Li, M. R. Gao, H. W. Liang, S. H. Yu, *ACS Nano* **2011**, *5*, 4211 – 4218.

[7] a) L. Wang, Y. Nemoto, Y. Yamauchi, *J. Am. Chem. Soc.* **2011**, *133*, 9674 – 9677; b) J. Anderson, A. Karakoti, D. J. Díaz, S. Seal, *J. Phys. Chem. C* **2010**, *114*, 4595 – 4602; c) B. Y. Xia, H. B. Wu, X. Wang, X. W. Lou, *J. Am. Chem. Soc.* **2012**, *134*, 13934 – 13937; d) S. Tominaka, M. Shigeto, H. Nishizeko, T. Osaka, *Chem. Commun.* **2010**, *46*, 8989 – 8991; e) Y. J. Kang, J. B. Pyo, X. C. Ye, T. R. Gordon, C. B. Murray, *ACS Nano* **2012**, *6*, 5642 – 5647; f) Z. m. Peng, H. J. You, H. Yang, *Adv. Funct. Mater.* **2010**, *20*, 3734 – 3741; g) C. K. Poh, Z. Q. Tian, J. J. Gao, Z. L. Liu, J. Y. Lin, Y. P. Feng, F. B. Su, *J. Mater. Chem.* **2012**, *22*, 13643 – 13652.

[8] a) S. E. Habas, H. Lee, V. Radmilovic, G. A. Somorjai, P. Yang, *Nat. Mater.* **2007**, *6*, 692 – 697; b) L. F. Liu, E. Pippel, R. Scholz, U. Gösele, *Nano Lett.* **2009**, *9*, 4352 – 4358.

[9] S. J. Guo, S. Zhang, X. L. Sun, S. H. Sun, *J. Am. Chem. Soc.* **2011**, *133*, 15354 – 15357.

[10] Y. Zhang, M. Janyasupab, C. W. Liu, X. X. Li, J. Q. Xu, C. C. Liu, *Adv. Funct. Mater.* **2012**, *22*, 3570 – 3575.

[11] a) C. H. Cui, H. H. Li, J. W. Yu, M. R. Gao, S. H. Yu, *Angew. Chem.* **2010**, *122*, 9335 – 9338; *Angew. Chem. Int. Ed.* **2010**, *49*, 9149 – 9152; b) C. H. Cui, H. H. Li, X. J. Liu, M. R. Gao, S. H. Yu, *ACS Catal.* **2012**, *2*, 916 – 924; c) C. H. Cui, H. H. Li, S. H. Yu, *Chem. Sci.* **2011**, *2*, 1611 – 1614.

[12] H. W. Liang, S. Liu, J. Y. Gong, S. B. Wang, L. Wang, S. H. Yu, *Adv. Mater.* **2009**, *21*, 1850 – 1854.

[13] a) H. W. Liang, X. Cao, F. Zhou, C. H. Cui, W. J. Zhang, S. H. Yu, *Adv. Mater.* **2011**, *23*, 1467 – 1471; b) C. Z. Zhu, S. J. Guo, S. J. Dong, *Adv. Mater.* **2012**, *24*, 2326 – 2331; c) C. Z. Zhu, S. J. Guo, S. J. Dong, *J. Mater. Chem.* **2012**, *22*, 14851 – 14855.

[14] a) J. H. Kim, S. M. Choi, S. H. Nam, M. H. Seo, S. H. Choi, W. B. Kim, *Appl. Catal. B* **2008**, *82*, 89 – 102; b) B. N. Wanjala, B. Fang, J. Luo, Y. Chen, J. Yin, M. H. Engelhard, R. Loukrakpam, C. J. Zhong, *J. Am. Chem. Soc.* **2011**, *133*, 12714 – 12727.

[15] C. X. Xu, Q. Li, Y. Q. Liu, J. P. Wang, H. R. Geng, *Langmuir* **2012**, *28*, 1886 – 1892.

[16] H. J. Wang, S. Ishihara, K. Ariga, Y. Yamauchi, *J. Am. Chem. Soc.* **2012**, *134*, 10819 – 10821.

[17] a) H. H. Li, C. H. Cui, S. Zhao, H. B. Yao, M. R. Gao, F. J. Fan, S. H. Yu, *Adv. Energy Mater.* **2012**, *2*, 1182 – 1187; b) M. Oezaslan, M. Heggen, P. Strasser, *J. Am. Chem. Soc.* **2012**, *134*, 514 – 524.

[18] C. H. Cui, X. J. Liu, H. H. Li, M. R. Gao, H. W. Liang, H. B. Yao, S. H. Yu, *ChemCatChem* **2012**, *4*, 1560 – 1563.

[19] X. G. Li, L. Y. Liu, J. W. Lee, B. N. Popov, *J. Power Sources* **2008**, *182*, 18 – 23.

[20] J. W. Guo, T. S. Zhao, J. Prabhuram, R. Chen, C. W. Wong, *Electrochim. Acta* **2005**, *51*, 754 – 763.

[21] a) D. Y. Wang, H. L. Chou, Y. C. Lin, F. J. Lai, C. H. Chen, J. F. Lee, B. J. Hwang, C. C. Chen, *J. Am. Chem. Soc.* **2012**, *134*, 10011 – 10020; b) P. Ferrin, M. Mavrikakis, *J. Am. Chem. Soc.* **2009**, *131*, 14381 – 14389.

[22] a) Y. Liu, M. F. Chi, V. Mazumder, K. L. More, S. Soled, J. D. Henao, S. H. Sun, *Chem. Mater.* **2011**, *23*, 4199 – 4203; b) Z. Q. Niu, D. S. Wang, R. Yu, Q. Peng, Y. D. Li, *Chem. Sci.* **2012**, *3*, 1925 – 1929; c) X. Zhao, M. Yin, L. Ma, L. Liang, C. P. Liu, J. H. Liao, T. H. Lu, W. Xing, *Energy Environ. Sci.* **2011**, *4*, 2736 – 2753; d) B. A. Kakade, T. Tamaki, H. Ohashi, T. Yamaguchi, *J. Phys. Chem. C* **2012**, *116*, 7464 – 7470.

